Spike-adding structure in fold/hom bursters

R. Barrio[a], S. Ibáñez[b], L. Pérez[b], S. Serrano[a]

[a] *IUMA and Dpto. Matemática Aplicada. Universidad de Zaragoza, E-50009 Zaragoza, Spain*
[b] *Departamento de Matemáticas. University of Oviedo, E-33007 Oviedo, Spain.*

Abstract

Square-wave or fold/hom bursting is typical of many excitable dynamical systems, such as pancreatic or other endocrine cells. Besides, it is also found in a great variety of fast-slow systems coming from other neural models, chemical reactions, laser dynamics, and so on. We focus on the spike-adding process and its connection with the homoclinic structure of the system. The creation of new fast spikes on a bursting neuron is an important phenomenon as it increases the duty cycle of the neuron. Here we mainly work with the Hindmarsh-Rose neuron model, a prototype of fold/hom bursting, but also with the pancreatic β-cell model, where, as already known from the literature, homoclinic bifurcations play an important role in bursting dynamics. Based on several numerical simulations, we present a theoretical scheme that provides a complete scenario of bifurcations involved in the spike-adding process and their connection with the homoclinic bifurcations on the parametric space. The global scheme explains the different phenomena of the spike-adding processes presented in literature (continuous and chaotic processes after Terman analysis) and moreover, it also indicates where each kind of spike-adding process occurs. Different elements are involved in the theoretical scheme, such as homoclinic isolas, canard orbits, inclination and orbit flip codimension-two bifurcation points and several pencils of period doubling and fold bifurcations, all of them illustrated with different numerical techniques. Some of these bifurcations needed in the process may be not visible on some numerical simulations because the organizing points are in different parametric planes due to the high dimension of the whole parameter space, but their effects are present. Therefore, we introduce a mechanism of the spike-adding process in fold/hom bursters in the whole space of parameters, even if apparently no role is played by the "far-away" homoclinic bifurcations. This fact is illustrated showing how the theoretical scheme provides a theoretical explanation to the different interspike-interval bifurcation diagrams (IBD) that have appeared in the literature for different models.

Keywords: spike-adding, fold/hom bursting, fast-slow dynamics, neuron models, homoclinic bifurcations
PACS: 87.19.ll, 05.45.-a
2000 MSC: 37Mxx, 37Gxx

1. Introduction

One of the most active research lines today is neuroscience, and a part of it is devoted to the study of its basic elements, neurons. Models in this field exhibit fast slow dynamics [1], a feature which is shared with many other models in practical applications as the case of some chemical reactions [2] or,

Email addresses: rbarrio@unizar.es (R. Barrio), mesa@uniovi.es (S. Ibáñez), perezplucia@uniovi.es (L. Pérez), sserrano@unizar.es (S. Serrano)

in the field of technology, laser devices [3]. An essential measure is the time that a neuron, or any other system, is active. This is related with the number of oscillations (spikes) in the fast subregime. In the literature there is a large number of articles dedicated to study the mechanisms involved in the spike-adding processes and also how the number of spikes change when one parameter is varied.

This paper studies the spike-adding process focusing on the Hindmarsh-Rose [4] neuron model, as a well known example and prototype of square-wave (or fold/hom) bursting [5]. Literature concerning this model is really impressive and, only in relation to our interests, we can quote [6, 7, 8, 9, 10, 11, 12, 13, 14, 15, 16, 17]. We contribute to the general understanding of the spike-adding process in fold/hom bursters, one of the most common ones. Namely, we put forward a theoretical scheme to describe the mechanisms involved in the formation of spikes in the context of such model. Later, we also show how these mechanisms are also observed in the Sherman et al. model of the pancreatic β-cell [18].

Since the pioneering work by Hodgkin and Huxley [19], many proposals have been made to encapsulate a qualitative description of the neuronal dynamics in a family of differential equations. The Hindmarsh-Rose model:

$$\begin{cases} \dot{x} = y - ax^3 + bx^2 - z + I, \\ \dot{y} = c - dx^2 - y, \\ \dot{z} = \varepsilon[s(x - x_0) - z], \end{cases} \tag{1}$$

is able to reproduce the most significant behaviours: quiescence, spiking and also bursting, either regular or irregular. Variable x represents the membrane potential, whereas y and z correspond to ionic currents. We consider a typical choice of parameters $a = 1$, $c = 1$, $d = 5$ and $s = 4$, discussing the spike-adding processes for different choices of the others [20]. The parameter ε is the small parameter of the model, giving rise to a fast-slow system with two fast and one slow variables.

This model is a prototypical example of fast-slow system. Bifurcations in the fast subsystem (limit case $\varepsilon = 0$) are essential elements of the fast-slow decomposition (first developed by Rinzel [21]) to explain the dynamics when ε is small. The study of the fast subsystem provides the spiking (or fast) manifold $\mathcal{M}_{fast}$, formed by stable limit cycles of the limit case, and the slow manifold $\mathcal{M}_{slow}$, formed by the equilibria of the limit case. The stable periodic orbits of the complete model behave following the well-known phenomenon, explained by singular perturbation theory and Fenichel's theorems [22], that the orbits (for small enough parameter ε) exhibit jumps from one manifold to the another one along its trajectory. Note that, when $\varepsilon = 0$, z is an additional parameter of system (1). Choosing b and I in suitable regions one can check that the curve of equilibrium points (slow manifold) exhibits a S-shape with two Hopf and fold bifurcations splitting the curve in stable and unstable branches (see [1] for more details).

We call bursting oscillation a time evolution consisting of bursts of rapid spikes (any excursion around the tubular manifold $\mathcal{M}_{fast}$), alternated by phases of relative quiescence (following $\mathcal{M}_{slow}$). The kind of bursting that we study here is said fold/hom [23] because the family of limit cycles displayed by the fast subsystem ends at a homoclinic bifurcation, where trajectories of the full system jump to the slow manifold.

By spike-adding process we understand any mechanism leading to the formation of additional turnings. The spiking rate and the time between spikes are essential elements in the understanding of the codifications in the neurons. As a result, spike-adding has been studied in many fold/hom neuron models [24, 25, 26, 27], including the Hindmarsh-Rose system as a prototypical one. It should be noted that in the literature one can find other types of spike addition processes that arise in bursting models of different nature, such as systems with external multiple frequency forcings, in which new bursting patterns can be observed [28, 29]. In these models, the effects of forcing frequencies must be taken into account. As well, phenomena of mixed mode burst oscillations (MMBO), that is, solutions that exhibit small amplitude oscillations and bursts consisting of one or multiple large amplitude oscillations, have been observed in some fourth order systems [10].

As explained in [30], the spike-adding transition may be either continuous, with a period which increases along the process, or discontinuous, involving chaotic phenomena. Relevance of fold bifurcations of periodic orbits was pointed out numerically in [31]. Dealing with fold/hom bursting, the spike-adding has also been related with canard orbits [14, 16, 32, 33], already anticipated in [30] when the increasing of the period was pointed out, and also with the existence of certain codimension-two homoclinic bifurcations [7, 8, 10, 16, 17]. Spike-adding cascades were also discussed in [25] for a modified version of the Hindmarsh-Rose model. Authors identified two different routes which were determined by the location of the equilibrium point in the full system with respect to the homoclinic bifurcation in the fast subsystem. One involves fold bifurcations of periodic orbits. In the second route the spike-adding cascade is organized by isolas.

As already mentioned, spike-adding mechanisms have been linked to the occurrence of certain codimension-two homoclinic bifurcations. Namely, fold and period doubling bifurcations have been shown to arise from codimension-two bifurcation points located along homoclinic bifurcation curves exhibited by the full system for fixed values of ε and with b and I varying. In this paper, we aim at showing the mechanism of the spike-adding process by proposing, based on our bifurcation results, a possible theoretical scheme that completes and provides answers to open questions related to the first scheme given in [16]. Moreover, the proposed scheme permits to locate theoretically both spike-adding processes studied by Terman [30], a connection which is missed in the literature.

All these spike-adding processes are usually illustrated by means of interspike-interval bifurcation diagrams (IBD) of stable bursting orbits as one parameter changes (see [9, 13, 25]). That kind of pictures shows different cascades of spike-adding (or period-adding) phenomena, crossing or not chaotic zones. The involved chaotic transitions have been discussed in several papers [8, 13, 15, 17], but what is missing is a connection with a theoretical framework. In Section 3 it is shown how the introduced global scheme provides a theoretical explanation to the different IBD diagrams that have appeared in the literature.

This paper is organized as follows. Section 2 presents a global three parametric numerical study of the Hindmarsh-Rose model focusing on the 2-3 spike-adding process (from 2 to 3 spikes per burst) and on the 6-7 one. Section 3 provides a theoretical scheme of the fold/hom spike-adding area with the different bifurcations involved in the process. Also, once the theoretical scheme is given we show how it provides an explanation for the typical IBD pictures shown in literature. An example using a more realistic model, the pancreatic β-cell neuron model of Sherman, Rinzel and Keizer (1988) [34], is presented in Section 4, showing that the same bifurcations as in the Hindmarsh-Rose model are present. Finally, we give some conclusions.

2. Global analysis

In this section we study the structure of the parametric space of the system by using different numerical techniques.

As an introduction, in Figure 1 we use the HR model to exemplify two processes of spike-adding usually shown in literature [13, 25]. Panel (a) shows an interspike-interval bifurcation diagram (IBD) of stable bursting orbits as I varies when $\varepsilon = 0.01$, $x_0 = -1$ and $b = 2.7$. Similar bifurcation diagrams are given in [9] where the spike-adding process is clearly shown. For high values of I, from right to left, the model exhibits tonic spiking which precedes a cascade of period doubling bifurcations leading to chaos. After crossing the chaotic zone the bifurcation diagram is wider and it starts an inverted cascade of period doubling bifurcations, and later a regular bursting regime with 12 spikes is observed. This transition is named a continuous interior crisis [11, 13] (compare also with [30] when Terman shows that a transition from n to $n+1$ spikes can be chaotic). When I decreases there is a sequence of spike-deletions between which there is a well-defined bursting regime. In [12, 13] it is said that the dynamics is block structured. Note that the transition between blocks can be again chaotic. As already mentioned, this type of diagram

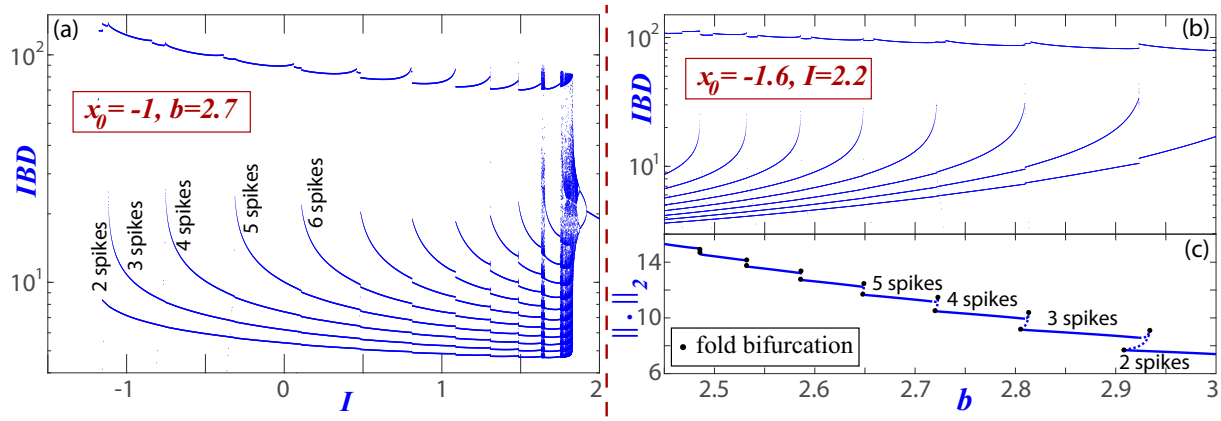

Figure 1: Two typical examples of spike-adding processes. Left: interspike-interval bifurcation diagram (IBD) with $x_0 = -1$, $b = 2.7$, $\varepsilon = 0.01$ and I as bifurcation parameter. Right: continuation of a periodic orbit with b varying and $x_0 = -1.6$, $I = 2.2$, $\varepsilon = 0.01$. This left panel shows the IBD and the $\|\cdot\|_2$ norm of the periodic orbit as a function of b, where solid (resp. dashed) refers to stable (resp. unstable) orbits.

is shown quite frequently in literature for different models but, although chaotic transitions are discussed, no connection with a theoretical framework is available.

Right side panel (b) shows another IBD. In this case b varies whereas $\varepsilon = 0.01$, $x_0 = -1.6$ and $I = 2.2$. From now on, unless indicated, we fix the value $x_0 = -1.6$. We also provide the continuation of a periodic orbit (plotting the $\|\cdot\|_2$ norm against b using AUTO continuation software [35]) along the whole process of spike-adding. Note that the periodic orbits evolve continuously with respect to the parameter (a similar evolution could be shown for the case of the left panel, at least for the transition from 2 spikes to 11 spikes). This spike-adding mechanism with a continuous evolution of the periodic orbit was already anticipated in [30]. Note that the sequence of bifurcations involved in the transition from n to $n+1$ spikes is always the same: two fold bifurcations give rise to an hysteresis phenomenon. These fold bifurcations are the key features of this spike-adding process. They have already been shown in some examples in [8, 14, 16].

As illustrated in Figure 1, spike-adding cascades determine, following the notion introduced in [13], a block structure in the bifurcation diagrams. But this analysis uses just one parameter, and other techniques are more suitable to provide results in higher parameter spaces. Figure 2 shows how these blocks give rise to bands when two- and three-parameter spaces are explored. Spike-counting technique [9], which counts the number of spikes in a burst, is used to obtain two-parameter sweeps on certain parameter planes: a vertical one with I fixed and five horizontal planes with ε fixed. Putting everything together on a three-dimensional parameter space (b, I, ε), we obtain the two pictures displayed in Figure 2 (front and back views). Clearly visualized, we observe a band structure which goes through a simplification process as ε increases: note how the number of colors (related with the number of spikes per burst) decreases. The simplification of the band structure is explained in [7] by means of a parallel process of simplification in the homoclinic structure in the system. The dark red regions denote chaotic areas or, due to the chosen color scale, they correspond to bursting orbits with a large number of spikes (see bottom part). For further understanding, one should place the bifurcation diagrams shown in Figure 1 in the context of Figure 2, where the IBD shown in the plot (b) of Figure 1 corresponds to a line in the three-parametric study of Figure 2 that crosses the different bands on the spike-adding process. Now the question is to focus on detecting the main ingredients that give rise to the structures observed in Figure 2.

In the sequel, we use the notation $hom^{(n,n+1)}$ to refer to a homoclinic bifurcation surface (or curve) where the homoclinic orbit evolves from n to $n+1$ spikes. In [6, 7], we showed how these homoclinic

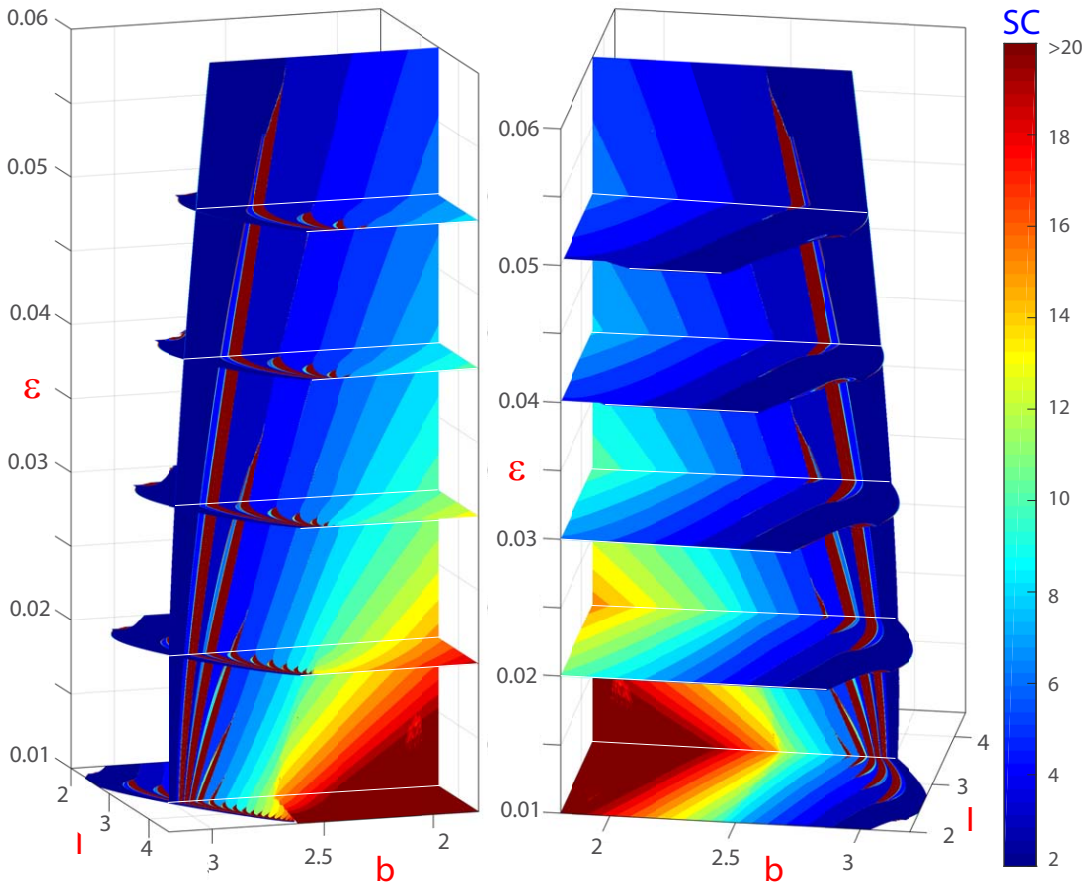

Figure 2: Three-parametric (b, I, ε) diagram showing the spike-counting (SC) sweeping technique, number of spikes per burst of the attractor, in different biparametric planes. The pictures show how the number of spikes per burst decreases when the small parameter ε grows and how less and less color bands appear. The global structure seems to be similar for any small value of the parameter, but with more color bands.

bifurcation surfaces overlap each other forming a structure of "mille-feuille". In turn, arising from these surfaces we find bifurcations of periodic orbits that are essential ingredients in the mechanisms of spike-adding. As already mentioned, bifurcations of periodic orbits involved in the spike-adding mechanisms in the Hindmarsh-Rose model were linked to the existence of certain codimension-two homoclinic bifurcations in [14, 16].

In Figure 3 we show bifurcation diagrams on parametric planes (b, I), fixing different values of ε. All of them show similar techniques and elements: spike-counting, a homoclinic bifurcation curve, codimension-two homoclinic bifurcation points, folds of periodic orbits and curves of period doubling bifurcation. Although three types of homoclinic bifurcations of codimension-two can appear, now we only pay attention to inclination flips (IF) and orbit flips (OF). In our case, at both bifurcations the linear part at the equilibrium point has real eigenvalues λ^s, λ^u and λ^{uu} with $\lambda^s < 0 < \lambda^u < \lambda^{uu}$. Passing through an inclination flip, the orientation of the global two-dimensional unstable manifold changes. Whereas through an orbit flip, there is a switching when, following the backward flow, the homoclinic orbit approaches the equilibrium over the leading unstable manifold; namely, the entrance branch is reversed. References [7] and [36] contain extended discussions regarding these codimension-two homoclinic bifurcations. There

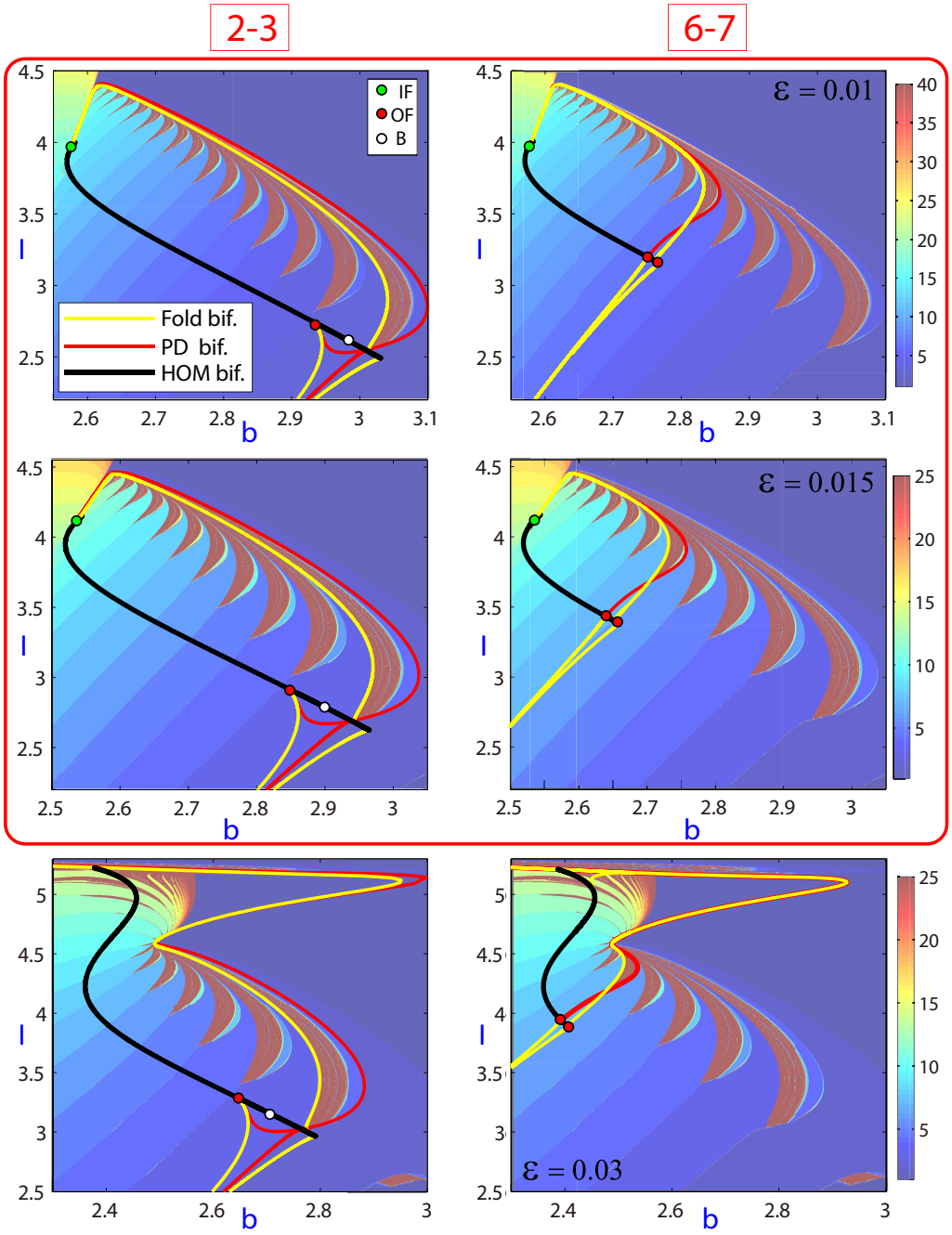

Figure 3: Three biparametric (b, I) spike-counting diagrams (for $\varepsilon = 0.01$, 0.015 and 0.03) and the main bifurcation lines detailed for the 2-3 and 6-7 spike-adding processes. The square remarked area shows the structure for small parameter values of ε (similar pictures for any $\varepsilon \ll 1$ exist but with more and more stripes). The PD and Fold bifurcations shown are the ones that delimit the spike-adding structure. Some codimension-2 homoclinic bifurcation points are marked on the corresponding homoclinic bifurcation lines. See the text for more details.

are three classes of flip homoclinic bifurcations: A, B and C. Those exhibited in the Hindmarsh-Rose model are all of type C. The corresponding theoretical bifurcation diagram is well-known in literature (see [36] and references therein). There exist pencils consisting of fold bifurcations of periodic orbits, period doubling bifurcations and wedge-shaped regions of chaotic behaviour.

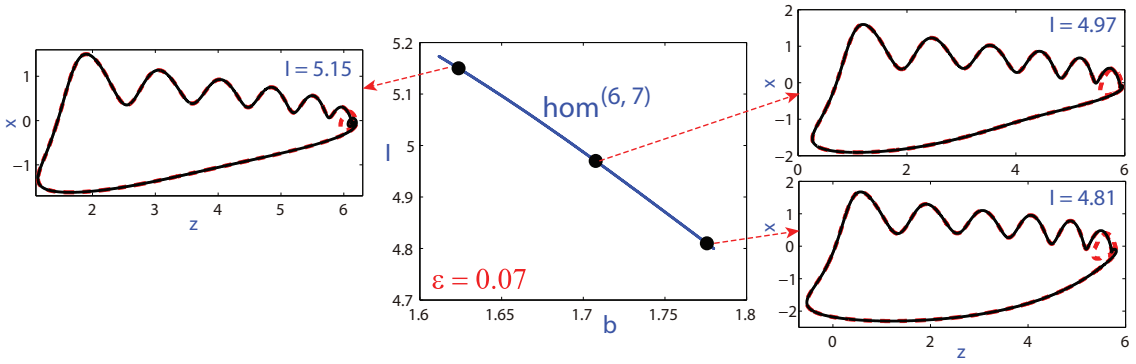

Figure 4: Center: Parameter plane (b, I) for $\varepsilon = 0.07$ showing the isola of the codimension-one homoclinic curve that gives 6-7 spikes per burst. Left and right: xz projections of two homoclinic orbits for three fixed values of I.

Left and right panels in Figure 3 show diagrams which include (black coloured lines) the curve $hom^{(2,3)}$ and $hom^{(6,7)}$, respectively. From top to bottom the values of ε are 0.01, 0.015 and 0.03. Note that, as already known from [16], the endpoints of the homoclinic bifurcation curve are only apparent ends. There, the curve is folded onto itself so that, actually, there is a double covering with two branches. In fact, it is argued in [7] that these curves are closed and hence it makes sense to refer to isolas limited by homoclinic bifurcations. To illustrate this fact, in Figure 4 we show (central panel) the curve $hom^{(6,7)}$ on the two-parameter plane (b, I) for $\varepsilon = 0.07$. It seems to be just a line, but this cannot be the case, as long as the bifurcation curve cannot stop suddenly, unless a codimension-two point or another singularity appears. If we follow the bifurcation curve with continuation techniques (using the software AUTO in our case) we really see that the continuation process produces foldings on the visible segment. To study what happens, we consider three values of the parameter I and we show the homoclinic orbits obtained in each one of the branches. At each value of I we have obtained two different homoclinic orbits (left and right panels in Figure 4). One has an extra loop around the equilibrium far from the burst activity, namely, there is a homoclinic orbit with six spikes (black color), and another one (red color) with seven spikes, but organized in two groups, one of six spikes and another one of just one. This provides a numerical evidence of the existence of the homoclinic isola.

In this paper we focus on small values of ε because we want to provide a study of the generic case when $\varepsilon \ll 1$. That is the reason why the bifurcation diagrams for $\varepsilon = 0.01$ and $\varepsilon = 0.015$ are remarked in Figure 3. Note that the main difference between small and large values of ε has to do with left ends of folds and period doubling bifurcations. Whereas for small values these curves emerge from inclination flip bifurcations placed on the left side of the homoclinic curve, for larger values these bifurcation curves extend far from the homoclinic structure.

To understand the theoretical scheme that we propose below in Section 3, one should pay attention to some of the differences observed in Figure 3. The most remarkable one is that, whereas $hom^{(6,7)}$ exhibits two orbit flips (OF), the left one located on the lower branch of the homoclinic curve and the right one on the upper one, $hom^{(2,3)}$ only exhibits one, located on the lower branch. We remark that the behaviour exhibited by $hom^{(6,7)}$ is the generic one, that is, it corresponds to the behaviour that we found along $hom^{(n,n+1)}$ for ε small and $n > 2$. Nevertheless, as already argued in [16], we stress that $hom^{(2,3)}$ behaves differently, although the global picture is similar, except in a very small region around the homoclinic

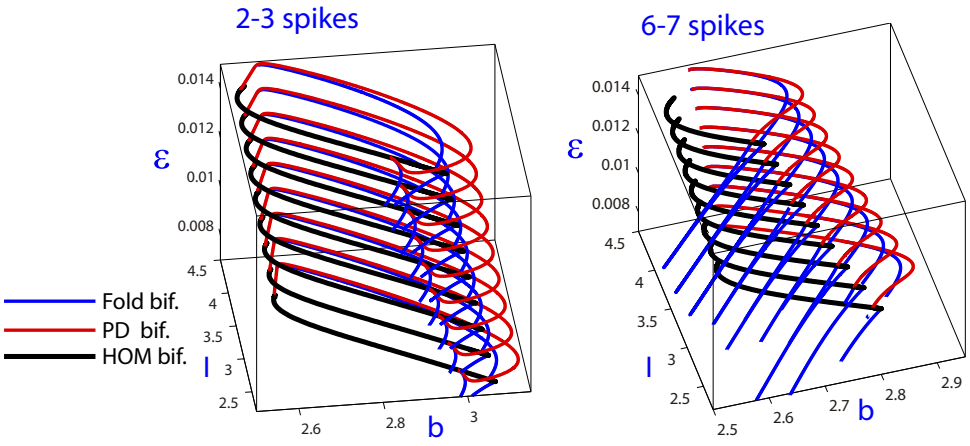

Figure 5: Three-parametric (b, I, ε) plots of homoclinic bifurcation curves corresponding to hom$^{(2,3)}$ and hom$^{(6,7)}$ for low values of the small parameter ε, including also the main PD and Fold bifurcations.

curve. We will come back to this later, when we discuss the scheme provided in Figure 6.

In Figure 5 we show that the structures observed in Figure 3 for some values of ε are the generic ones for ε small enough. The bifurcation curves build up surfaces in the three-parameter space (b, I, ε). Later on, this global structure will allow us to understand, from a slightly different perspective, the different explorations on spike-adding processes provided in the literature.

3. Global theoretical scheme

In Section 2 we have seen numerically how the main bifurcations (period doublings and folds of periodic orbits) which are involved in the spike-adding mechanism are organized with respect to the homoclinic structures exhibited in the system. Next, we introduce a theoretical scheme providing a fully general overview of the process.

3.1. Global theoretical scheme: biparametric case (ε fixed)

Using the numerical simulations shown in Section 2 and previously in [7, 8, 16], we provide in Figure 6 a more complete generic scenario of the transition in fold/hom bursters from n to $n+1$ spikes when ε is small. Note that the homoclinic isola component was illustrated in the previous section exploring the $hom^{(6,7)}$ case. As already explained in [7], the homoclinic isolas are piled up and their size decreases as the number of spikes increases. In each homoclinic curve we find some significant degenerations: three inclination flips and two orbit flips. The two inclination flips on the left side are terminal points for fold and period doubling bifurcations, but they do not play a relevant role in the discussion below. Depending on the location, either above or below the isola, the mechanisms to create extra spikes are different. Note that the scheme is partial as more bifurcations and codimension-two points should be present.

In Figure 6 we have remarked the complete structure for the n to $n+1$ ($n > 2$) spike-adding process. Suppose we follow the evolution of a periodic orbit with n spikes as we move from the right side of the parameter plane and below the homoclinic curve (see right plots of Figure 1). This orbit undergoes through two fold bifurcations which give rise to a hysteresis phenomena (a Z-shaped continuation curve). The first one is on the left, where the orbit becomes unstable and later the continuation goes back to the right till the fold bifurcation on the right is reached. There, the periodic orbit becomes stable again and, as we will shortly explain, exhibits an extra spike. The stability is lost later through several period

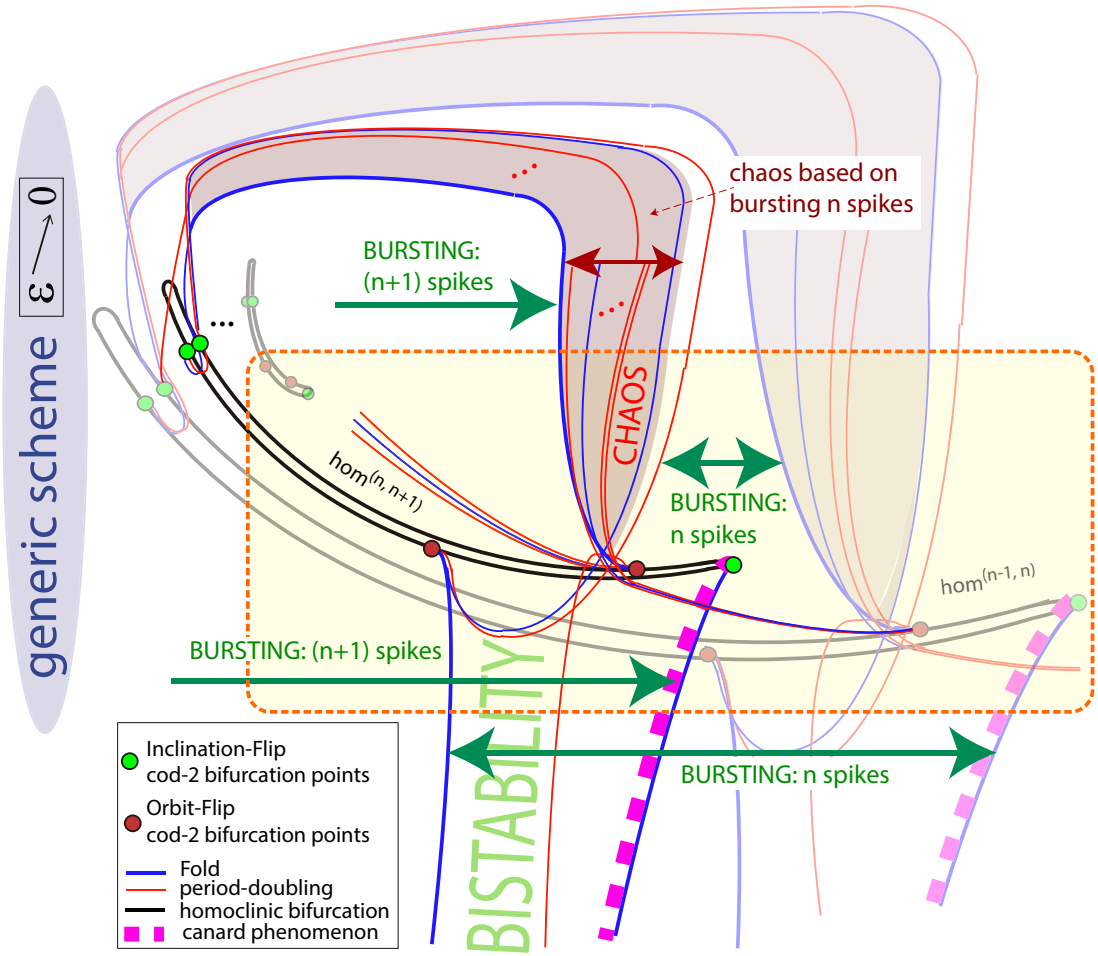

Figure 6: Generic theoretical scheme ($n > 2$) showing the entwined bifurcation diagram involved in the spike-adding mechanisms. See the text for explanation.

doubling and fold bifurcations (due to some pencils of these bifurcations generated on codimension-two bifurcation points) till another period doubling, located in between both main fold bifurcations, is reached. Hysteresis explains the existence of a region of bistability, where orbits with n spikes coexist with orbits with $n+1$ spikes. The addition of the extra spike is explained by a canard transition [10, 14] which occurs while the orbit undergoes through the second fold bifurcation on the right side. On the other hand, the transition from n to $n+1$ spikes above the homoclinic isola involves a chaotic region. Note that the theoretical scheme includes the two types of spike-adding processes introduced by Terman in [30] and also described in [13, 14, 16]. The main original contributions of the scheme are, first to establish what areas will produce each kind of spike-adding, and second to provide an overall explanation of the origin of the bifurcations involved in each type of spike-adding process. Later, in Figure 8, we will provide numerical explorations to illustrate both, continuous and chaotic spike-adding processes. We remark that the boxed area of Figure 6 contains the main ingredients for the spike-adding process in a fold/hom burster (as it is shown later in Section 4 for the pancreatic β-cell model), while the complete panel explains the complete structure for the Hindmarsh-Rose model.

Next, we describe in detail the location of the codimension-one bifurcations of periodic orbits proposed in Figure 6. Let us first pay attention to the bifurcations involved in the continuous spike-adding process (below the homoclinic isola). The fold bifurcation on the left emerges from the orbit flip on the left, located on the lower branch of the homoclinic curve. At this orbit flip the homoclinic connection exhibits n spikes. This fits with the fact that, at the fold bifurcation on the left, the periodic orbit also has n spikes. On the other hand, the fold bifurcation on the right emerges from an inclination flip located on the folding of the homoclinic isola [16]. Note again that this fits with the fact that at this fold bifurcation the periodic orbit is still evolving from n to $n+1$ spikes. Indeed, as we will illustrate later in Figure 9, while the periodic orbit undergoes through the fold bifurcation on the right the head of a canard orbit is starting to develop and, as a consequence, an extra spike is being formed. It makes sense to think that this mechanism is related to its counterpart behaviour along the homoclinic curve. In addition, as we will see later, the existence, conjectured in [16] but not numerically detected (due to precision limitations of any available numerical continuation software), of the inclination flip on the folding of the homoclinic isola, is explained by arguments related to the form in which periodic orbits are created from the homoclinic curve. On the other hand, the chaotic lobe is related to several codimension-two homoclinic bifurcations. The fold and period doubling bifurcations at the right, separating the chaotic zone from the region corresponding to bursting with n spikes, emerge from the orbit flip located on the lower (n-spikes) branch of $hom^{(n,n+1)}$. The fold bifurcation at the left, that is, the frontier between the chaotic zone and the region corresponding to bursting with $n+1$ spikes, emerges from the orbit flip located on the upper ($n+1$ spikes) branch of $hom^{(n,n+1)}$. In Figure 8 we will show that the chaotic behaviour inside the upper chaotic lobe is based on bursting behaviour with n-spikes, and so the pencils of bifurcations associated with that phenomena have to be generated on a codimension-two point related with n-spikes behaviour. Therefore, we conjecture that the period doubling and fold bifurcations inside the chaotic lobe emerge from the orbit flip located on the upper branch (n-spikes) of the previous homoclinic curve $hom^{(n-1,n)}$.

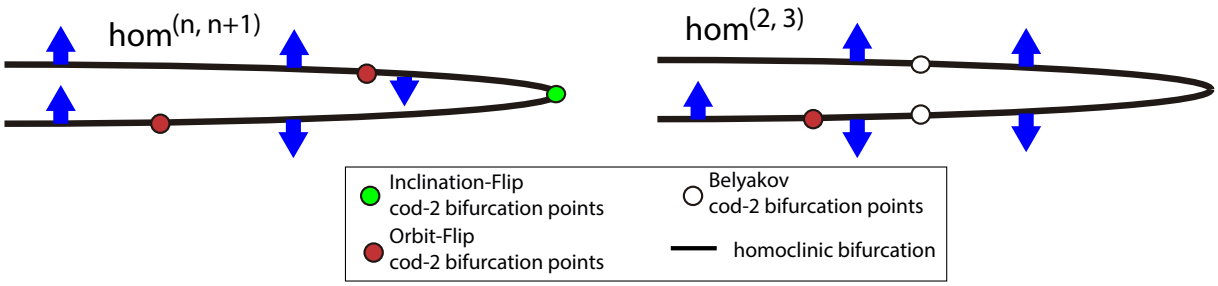

Figure 7: Directions in which the saddle periodic orbits emerge from the homoclinic connection as we move along the homoclinic bifurcation curve. In the generic case ($n > 2$) there are three changes of direction, two of them are explained by the existence of orbit flips, whereas, the other can be explained by the presence of an inclination flip. In the case of the curve $hom^{(2,3)}$ there is only one change which is explained by the existence of just an orbit flip.

As already mentioned, AUTO is not able to detect the inclination flip located at the right end of the isolas. Nevertheless, as reasoned in [16], there is an argument to show that there must be another degeneracy in between the orbit flips when we move from one to the other side of the isola along the right side of the curve. Arrows in Figure 7 indicate the direction in which single saddle periodic orbits emerge [37] from the homoclinic bifurcation curve (determined using AUTO software). Left panel shows the generic case where we see that there are, at least, three changes of direction. Following [16, 38], there are three codimension-two homoclinic bifurcations which can explain the side-switching: orbit flip, inclination flip and resonant eigenvalues. The latter one is excluded and moreover, following the homoclinic orbit from one orbit flip to the other along the right side, there is no change in the direction along which the homoclinic orbit leaves the equilibrium point and, hence, no additional orbit flip may exist in between.

The only option to explain the change in the direction of the arrows is the existence of an inclination flip. The same situation can be found in literature in a different model [38].

Right panel in Figure 7 corresponds to the curve $hom^{(2,3)}$. In this case only one change of direction is observed. This fits with the fact that in this case (and also along $hom^{(1,2)}$) only one orbit flip exists. In fact, the existence of an inclination flip at the right tip of the isola in these two cases is discarded because there exist two Belyakov bifurcation points and the right side of the homoclinic curve in between the Belyakov points corresponds to saddle-focus equilibrium points and so, flip bifurcations make no sense.

We remark that our theoretical scheme of Figure 6 is valid for the generic case of $hom^{(n,n+1)}$ with $n > 2$. As already explained, in the generic case, one of the fold bifurcations involved in the continuous spike-adding emerges from the inclination flip at the tip on right side of the homoclinic isola, as well as one of the folds involved in the chaotic spike-adding emerges from the orbit flip located on the upper branch of the curve $hom^{(n,n+1)}$. When $n = 2$, there are only one OF point on the lower branch of the curve $hom^{(2,3)}$. In any case, the macroscopic global view is similar to the generic case, as shown in Figure 3.

Both cases, continuous and chaotic spike-adding transitions, are illustrated in Figure 8 for the case of the transition from 2 to 3 spikes (we have chosen this case as globally the process is the same but it is easier and better visualized due to the bigger area involved). A periodic orbit is continued along three different segments of parameters: L_1, L_2 and L_3 as displayed in the top panel. Bottom panels show the corresponding bifurcation diagrams: on the vertical axis we plot the value of y (top diagrams) at the points where the variable x has a maximum and the $\|\cdot\|_2$ norm (bottom diagrams) of the periodic orbit.

Along the segment L_1 we observe a continuous spike-adding process. From right to left, we see how a periodic orbit with 2 spikes undergoes a fold bifurcation at which it looses its stability. Later, now for b moving to right, the periodic orbit increases its length until it reaches a second fold at which b starts to decrease again. The periodic orbit recovers the stability after a period doubling bifurcation. Note that in this area there are pencils of bifurcations very close each other, and so it is quite difficult to observe them and their effects. Just to show this, the doubled periodic orbit emerging at that point ($b \simeq 2.922$) is also continued with AUTO. It undergoes through a fold bifurcation where parameter b starts to increase until a second period doubling is reached, and so on (note that the unstable orbit is connected with bifurcated orbits close to the fold on the right). This process only can be detected using continuation techniques because the stable region is very small and it has no real effects in the dynamics.

The behaviour along the segment L_2, very close to the homoclinic curve but below, exhibits some differences to that already described along the segment L_1, but the process is still continuous. The main difference is that in this case there is a microchaotic structure coexisting with stable periodic orbits due to the segment L_2 crosses pencils of period doublings and fold bifurcations generated on the orbit flip point located on the left (see [8] for additional details).

Finally, along the segment L_3, the spike-adding process is discontinuous, going through a chaotic area. Starting from the right we see how a 2-spikes periodic orbit goes through a chaotic window after which only one stable orbit persists, but exhibiting 3 spikes. Note that the chaotic window is generated via a period doubling cascade originated from a bursting orbit with 2 spikes, as shown on the picture on the right for the segment L_3. Note that the determining characteristic for the process of spike-adding to be continuous or discontinuous is on which side of the homoclinic curve the system is located and, therefore, what are the bifurcations that affect it.

A picture of the transition from 2 to 3 spikes along the segment L_1 is given in Figure 9. Following the bifurcation curve depicted in the plane $(b, \|\cdot\|_2)$ displayed in the right panel, the excursion starts on the lower branch of the bifurcation curve where the 2-spikes periodic orbit is stable. After undergoing through a fold bifurcation, the periodic orbit becomes unstable and its length starts to increase as b decreases. This is the beginning of the canard transition already mentioned. The increment in the length of the periodic orbit occurs as it extends following the piece of the slow manifold. The orbit evolves from

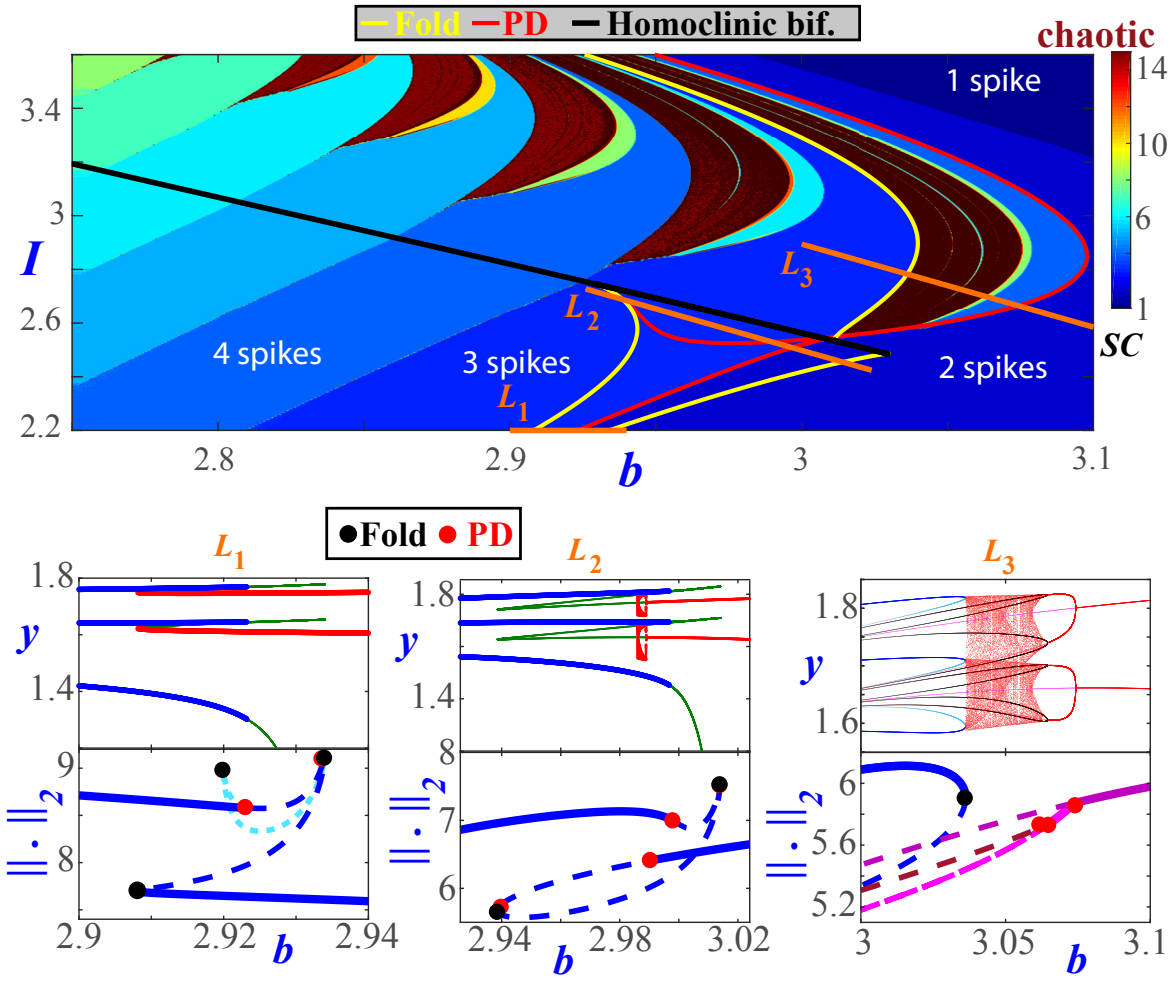

Figure 8: Analysis of the spike-adding process from 2 to 3 spikes for $\varepsilon = 0.01$. Top: Biparametric diagram with the spike-counting technique and main bifurcation curves for the transition along selected spike-adding process. Bottom: Bifurcation diagrams for segments marked on top picture ($L_1 \equiv I = 2.2$; $L_2 \equiv I = 2.727 - 3.0918(b - 2.926)$; $L_3 \equiv I = 2.891 - 3.0918(b - 3.001)$). Two pictures have been performed for each segment: one plot with the standard bifurcation continuation diagram given by AUTO showing the $\|\cdot\|_2$ norm of the orbit and another one with the y value of the points where the corresponding orbit has a maximum for variable x.

"headless" canard to a maximal canard, giving finally a bursting orbit with an extra spike (for details, see [10, 14]). Homoclinic orbits undergo similar transformations as they evolve from the orbit flip located in the lower branch of the homoclinic curve and they pass the right-folding (see [16] for an example showing the transition from 3 to 4 spikes).

3.2. Global theoretical scheme: global case

The structure provided by the theoretical scheme is robust with respect to ε for small values of this parameter. In Figure 10 the theoretical scheme of Figure 6 is visualized into a three-parameter space. Note that the surfaces of fold bifurcation and period doubling involved in the spike-adding process emerge from the homoclinic bifurcation curves. A green plane is marked to emphasize that, in principle, it would

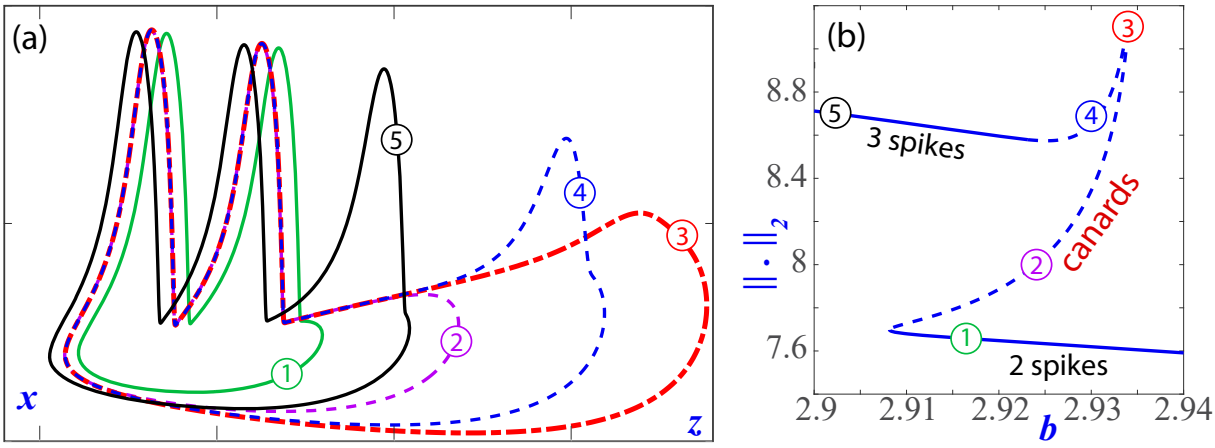

Figure 9: (a): Evolution of periodic orbits throughout the process of spike-adding. (b): Bifurcation diagram obtained by continuation corresponding to the segment L_1 on Figure 8. The coloured numbers mark the points in the diagram corresponding to the selected values. Along the continuation of the bifurcation lines we observe periodic orbits with two spikes (orbit 1), later headless canards (orbit 2), maximal canard (orbit 3), canards with head (orbit 4), and finally orbits with three spikes (orbit 5).

be possible to take two-parameter slides hiding the whole homoclinic structure, but in any case, as we have argued, the spike-adding process cannot be fully understood without realizing the full bifurcation diagram. Particularly, all previous explorations recorded in the literature fit with our scheme, although in some of them it is not possible to see any homoclinic bifurcation (it depends on the selected parameters and regions as argued from Figure 10). In fact, all the situations detected in previous studies can be explained with a single global theoretical scheme shown in Figure 10.

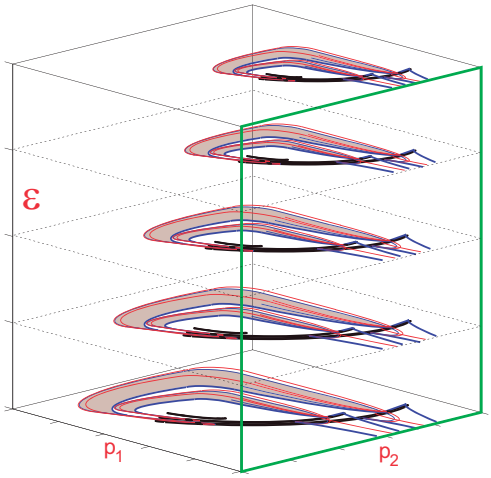

Figure 10: Scheme of a three-dimensional view of the theoretical scheme (only essential elements are displayed). The structure persists for small values of ε.

In order to see how the theoretical scheme given in Figure 6 is valid for the classical 1D views provided in literature, we take again the pictures of Figure 1. Plots (b) and (c) have been already studied in Figures 8 and 9 linking them with the results of Figure 6. Now, we intend to explain the theoretical

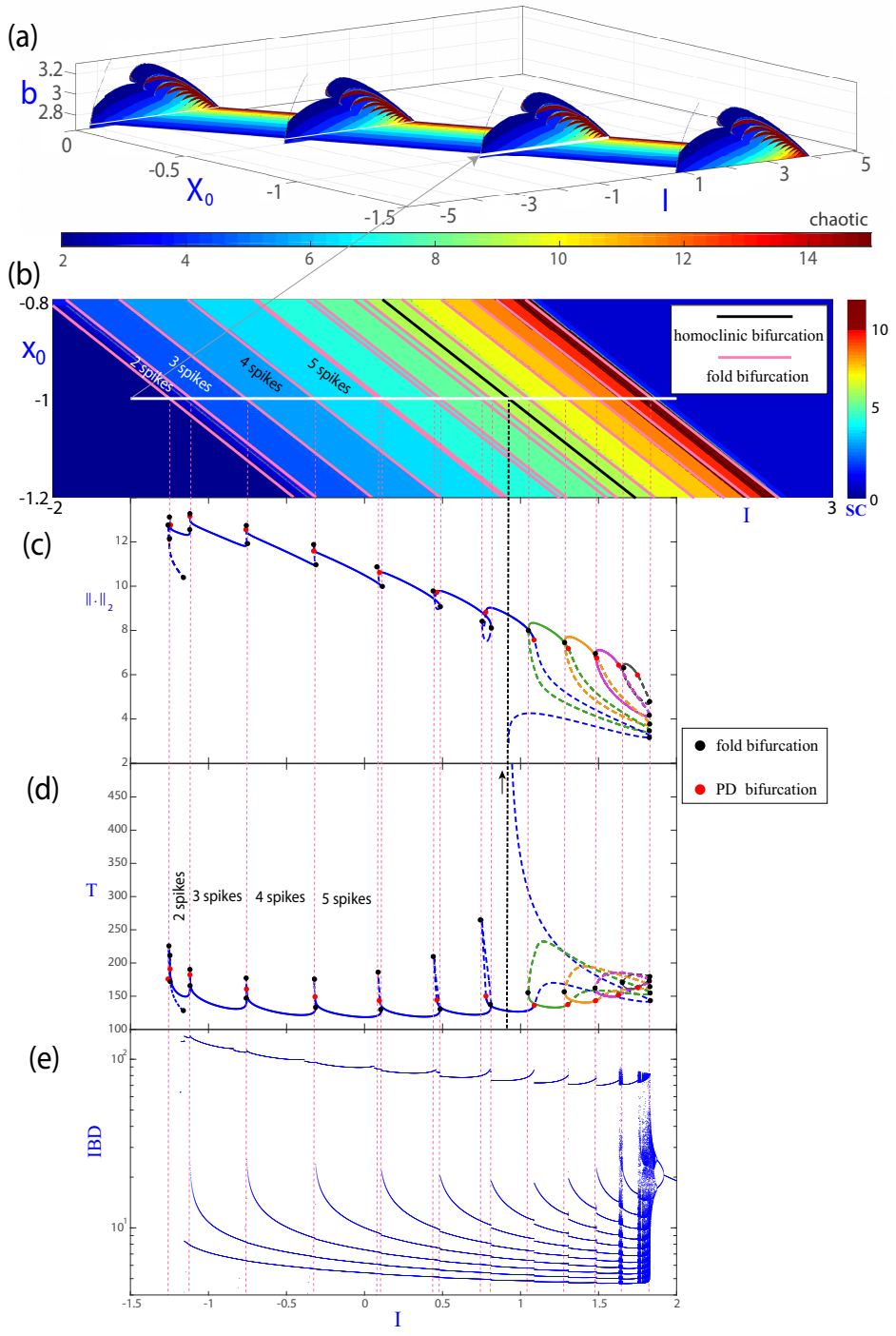

Figure 11: (a) Three-parametric (I, x_0, b) diagram showing the spike-counting (SC) sweeping technique in different biparametric planes using $\varepsilon = 0.01$. (b) Biparametric (I, x_0) diagram with $b = 2.7$. And (c), (d) and (e), 1D cuts on the line $x_0 = -1$ showing the $\|\cdot\|_2$ norm, the period and the IBD of the orbit, respectively. Several bifurcation lines and points are depicted.

facts of the 1D simulation shown on plot (a) of Figure 1 (we recall that this type of 1D visualization was already considered in [9, 13], among others). Top panel in Figure 11 shows how the three-parametric global scheme does not only extends adding ε but also other parameters as, for instance, x_0 (compare also with Figure 2). In this case we observe that moving parameter x_0 just makes a translation of the global picture in the parameter space, and therefore the biparametric picture (I, x_0) just shows a parallel band structure as presented in plot (b). On that picture we also add some bifurcation lines (fold and homoclinic bifurcations), that obviously follow the band structure, giving straight lines. Taking now a segment fixing $b = 2.7$, $x_0 = -1$ and $\varepsilon = 0.01$ as that depicted in panel (b), we obtain the bifurcation diagrams displayed in panels (c), (d) and (e). Note that plot (e) corresponds to the IBD right panel of Figure 1.

It is important to remark that when one studies the interspike-interval bifurcation diagram shown in panel (e), and we note that this is the most standard visualization of this kind of systems in literature, the relevance of the homoclinic bifurcation remains hidden, in spite of the segment crosses the homoclinic surface. In order to reveal the internal structure of the spike-adding process in that line, we need to use continuation techniques. To that goal, we pay now attention to the other two 1D bifurcation diagrams of panels (c) and (d), where we show the $\|\cdot\|_2$ norm and the period of the stable (continuous line) and unstable (discontinuous line) periodic orbits for the given parametric values computed using AUTO software. Starting from the left, we see that there exists a spike-adding cascade, but moving to the right, the role of the homoclinic orbit is again hidden because we are now following the stable branch of periodic orbits. Only when we continue the orbit up to the last fold bifurcation we see that an unstable periodic orbit persists as I decreases up to it undergoes a homoclinic bifurcation on the value marked by a dotted vertical line. So, attending to this exploration, we can say that it is at the homoclinic orbit where the periodic orbit involved in the continuous spike-adding is created, but when the periodic orbit bifurcates from the homoclinic orbit it is unstable and only recovers the stability through period doubling or fold bifurcations.

Note that to the right of the homoclinic bifurcation the spike-adding is chaotic: the segment crosses chaotic lobes, most of them very narrow, and so difficult to detect. In that region the bands of periodic orbits with a fix number of spikes are in fact formed by isolas of periodic orbits disconnected one each other. The periodic orbits experiment a period doubling cascade (we just depict the first period doubling with a red dot) generating the chaotic region. One should also compare with the continuation along the segment L_3 in Figure 8. Recall that, when explained by a chaotic process, the spike-adding is discontinuous (see [30]). Discontinuities are apparent in the inter-spike interval bifurcation diagram depicted in Figure 11 (panel (e)). In panels (c) and (d) we observe that the bifurcation curves emerging from the cascade of folds located to the right of the homoclinic bifurcation create isolas with a fold bifurcation point located to the right side of the bifurcation diagram. In fact, close to the value of I for which the segment enters in the region with one spike, there is a collection of fold bifurcation curves. Note that all of these bifurcation points are in fact the intersection with the pencils of bifurcations created on the orbit-flip and inclination-flip points located on the homoclinic bifurcation curve but on different parametric planes.

Finally, we remark that the global scheme presented in this paper explains most of the phenomena of the spike-adding process as it relates the different bifurcation lines, that are present in Figures 8 and 11, with the pencils of bifurcations created on the codimension-two homoclinic bifurcation points that are in different parametric planes and that cannot be seen in the selected set of parameters. As illustrated on Figure 10, when we have a large parametric phase space, it depends on how and where we make a section in order to better visualize the real organizing points of the studied phenomena.

4. Pancreatic β-cell neuron model

In this section we briefly illustrate that similar structures, as the ones observed for the Hindmarsh-Rose neuron model, are observed in other fold/hom neuron bursting models. Different models of pancreatic β-cells are usually based on the standard Hodgkin-Huxley formalism including different phenomena [34, 39, 40], like the intracellular storage of Ca^{2+}, the glucose metabolism, the influence of ATP, and so on. The most simple model of pancreatic β-cells which generates a realistic bursting behaviour is a three-dimensional model with two fast variables and one slow variable. In this paper we consider the model of Sherman, Rinzel and Keizer (1988) [34] given by

$$\left\{\begin{array}{rcl} \tau\dot{V} &=& -[I_{Ca}(V) + I_K(V,n) + g_S S(V - V_K)] + I_{app}, \\ \tau\dot{n} &=& \sigma[n_\infty(V) - n], \\ \tau_S\dot{S} &=& S_\infty(V) - S, \end{array}\right. \tag{2}$$

with the auxiliary ionic current functions defined by I_{app} (the external current) and

$$I_{Ca}(V) = g_{Ca}\, m_\infty(V)\,(V - V_{Ca}), \qquad I_K(V,n) = g_K\, n\,(V - V_K),$$

and where the different steady state gating variables take the forms

$$m_\infty(V) = \left[1 + \exp\left(\frac{V_m - V}{\theta_m}\right)\right]^{-1}, \quad n_\infty(V) = \left[1 + \exp\left(\frac{V_n - V}{\theta_n}\right)\right]^{-1},$$
$$S_\infty(V) = \left[1 + \exp\left(\frac{V_S - V}{\theta_S}\right)\right]^{-1}.$$

In this model, V represents the membrane potential, n the opening probability of the potassium channels and I_{Ca} and I_K are the calcium and potassium currents, (for more details see [27, 34]). The fixed parameters values that we use are taken from reference [27] and they are given by

$$\begin{array}{lllllll} \tau = 0.02, & \tau_S = 5, & V_{Ca} = 25, & V_K = -75, & g_{Ca} = 3.6, & g_K = 10.0, & g_S = 4, \\ \sigma = 0.85, & V_m = -20, & V_n = -16, & \theta_m = 12, & \theta_n = 5.6, & \theta_S = 10. & \end{array}$$

The ratio $k_S = \tau/\tau_S$, in our case $k_S = 0.004$, defines the ratio of the time parameters for the fast (V and n) and the slow (S) variables. The parameter V_S is the main bifurcation parameter and it defines the membrane potential at which the steady-state value for the gating variable S attains one-half of its maximum value.

In Figure 12 we show bifurcation diagrams on the parametric plane (V_S, I_{app}). These pictures are similar to the ones shown in Figure 3 for the Hindmarsh-Rose model. The main difference is that for this model it is much more difficult to locate numerically the different elements that are clearly shown in the Hindmarsh-Rose model. Besides, in the β-cell neuron model we do not have Belyakov points for the 2-3 spike-adding process, and so now this case also follows the generic theoretical scheme of the boxed area of Figure 6 with two orbit flip codimension-two points. As in the Hindmarsh-Rose model, an inclination flip point is conjectured in the sharp fold of the homoclinic curves. The 2-3 spike-adding process is detailed with a magnification of the bifurcation lines. On the left side of the homoclinic curve the main fold bifurcations that create the spike-adding region go to one OF and to the conjectured IF. On the right side, the period doubling and fold bifurcation lines that delimit the chaotic lobe go each one to different OF points as shown in the generic theoretical scheme of Figure 6. On the magnification on Figure 12 the continuous lines are the ones computed with AUTO, and the discontinuous ones are the conjectured continuation of the lines.

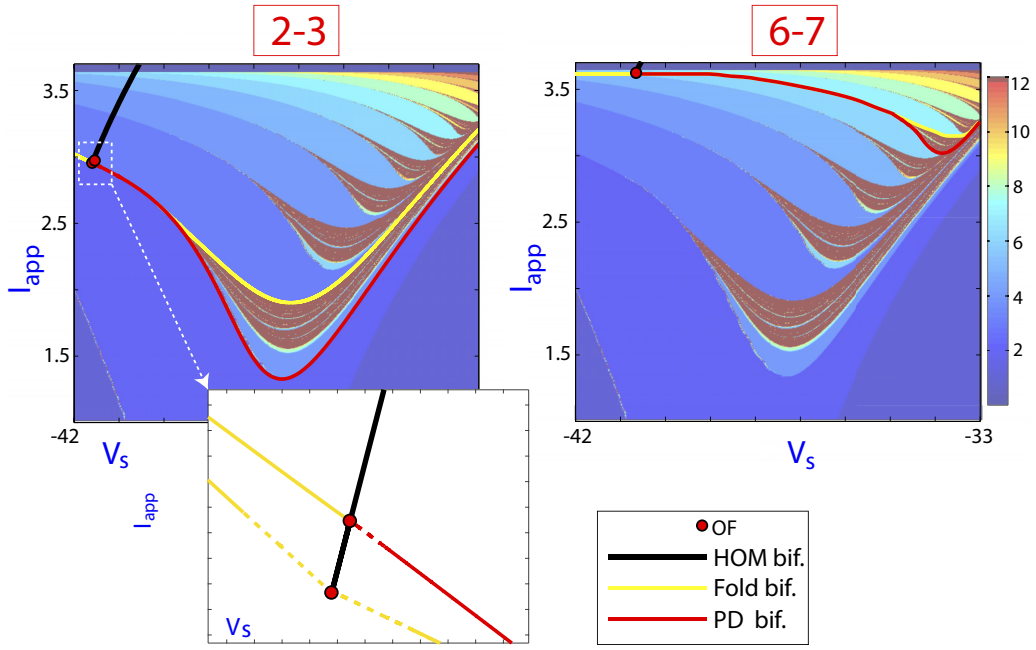

Figure 12: Biparametric (V_S, I_{app}) spike-counting diagrams of the β-cell neuron model (for $k_S = 0.004$) and the main bifurcation lines detailed for the 2-3 and 6-7 spike-adding processes. Some codimension-2 homoclinic bifurcation points are marked on the corresponding homoclinic bifurcation lines. See the text for more details.

On the 6-7 spike-adding process the numerical continuation software is not able to compute some of the curves close to the codimension-two points (AUTO detects the two OF points, but they are very close each other).

Therefore, from this brief analysis on the β-cell neuron model, it is plausible that the fold/hom spike-adding process in mathematical neuron models follows the theoretical scheme shown in Figure 6. Note that the Figure 6 provides the complete scheme for the Hindmarsh-Rose model, while the boxed area the generic scheme for fold/hom bursters. The great advantage of using the Hindmarsh-Rose model is that it makes more easy to detect the different elements of the spike-adding process.

Conclusions

We propose a global scheme to understand the spike-adding process in fold/hom bursting models, exemplified in the Hindmarsh-Rose neuron model. In the analysis we use different numerical techniques such as spike-counting, Lyapunov exponents and bifurcation continuation methods. Our simulations, and those of literature, allow us to introduce a global theoretical scheme that completes the previous ones that appeared recently (see [16]). The global framework connects the different types (continuous and chaotic) of spike-adding processes introduced by Terman [30]. It determines the regions of the parametric space where each kind of process occurs, and provides a general explanation of the origin of the bifurcations involved in them. Finally, being a global and multiparametric scheme, it allows to give an explanation to the different interspike-interval bifurcation diagrams (IBD) that have appeared in the literature for different models. This is an important point, since in most papers the spike-adding process is illustrated only with IBD plots, but without connecting to any region or bifurcation. In addition, an example has been presented that uses a more realistic model, the pancreatic β-cell neuron model of Sherman et al.,

which shows the same scheme as in the Hindmarsh-Rose model. Therefore, there are indications of the universality of this theoretical scheme for the generic fold/hom spike-adding process.

Acknowledgments

RB and SS have been supported by the Spanish Research projects MTM2015-64095-P, PGC2018-096026-B-I00, the Universidad de Zaragoza-CUD project UZCUD2019-CIE-04 and European Regional Development Fund and Diputación General de Aragón (E24-17R and LMP124-18). SI and LP have been supported by Spanish Research projects MTM2014-56953-P and MTM2017-87697-P. LP has been partially supported by the Gobierno de Asturias project PA-18-PF-BP17-072.

Bibliography

[1] G. B. Ermentrout, D. H. Terman, Mathematical foundations of neuroscience, Vol. 35 of Interdisciplinary Applied Mathematics, Springer, New York, 2010.
[2] M. Broens, K. Bar-Eli, Canard explosion and excitation in a model of the Belousov-Zhabotinskii reaction, The Journal of Physical Chemistry 95 (22) (1991) 8706–8713.
[3] S. Wieczorek, B. Krauskopf, D. Lenstra, Multipulse excitability in a semiconductor laser with optical injection, Phys. Rev. Lett. 88 (2002) 063901.
[4] J. L. Hindmarsh, R. M. Rose, A model of the nerve impulse using three coupled first-order differential equations, Proc. Roy. Soc. Lond. B221 (1984) 87–102.
[5] E. M. Izhikevich, Neural excitability, spiking and bursting, Int. J. Bifur. Chaos Appl. Sci. 10 (06) (2000) 1171–1266.
[6] R. Barrio, S. Ibáñez, L. Pérez, Hindmarsh-Rose model: close and far to the singular limit, Phys. Lett. A 381 (6) (2017) 597–603.
[7] R. Barrio, S. Ibáñez, L. Pérez, Homoclinic organization in fold/hom bursters: the Hindmarsh-Rose model, Preprint.
[8] R. Barrio, M. A. Martínez, S. Serrano, A. Shilnikov, Macro- and micro-chaotic structures in the Hindmarsh–Rose model of bursting neurons, Chaos 24 (2) (2014) 023128.
[9] R. Barrio, A. Shilnikov, Parameter-sweeping techniques for temporal dynamics of neuronal systems: case study of Hindmarsh-Rose model, Journal of Mathematical Neuroscience 1 (2011) 6:1–6:22.
[10] M. Desroches, T. J. Kaper, M. Krupa, Mixed-mode bursting oscillations: Dynamics created by a slow passage through spike-adding canard explosion in a square-wave burster, Chaos 23 (4) (2013) 046106.
[11] J. M. González-Miranda, Observation of a continuous interior crisis in the Hindmarsh-Rose neuron model, Chaos 13 (3) (2003) 845–852.
[12] J. M. González-Miranda, Block structured dynamics and neuronal coding, Physical Review E 72 (2005) 051922.
[13] J. M. Gonzalez-Miranda, Complex bifurcation structures in the Hindmarsh-Rose neuron model, Int. J. Bifur. Chaos Appl. Sci. 17 (2007) 3071.
[14] G. Innocenti, A. Morelli, R. Genesio, A. Torcini, Dynamical phases of the Hindmarsh-Rose neuronal model: Studies of the transition from bursting to spiking chaos, Chaos 17 (4) (2007) 043128.
[15] G. Innocenti, R. Genesio, On the dynamics of chaotic spiking-bursting transition in the Hindmarsh—Rose neuron, Chaos 19 (2) (2009) 023124.
[16] D. Linaro, A. Champneys, M. Desroches, M. Storace, Codimension-two homoclinic bifurcations underlying spike adding in the Hindmarsh-Rose burster, SIAM J. Appl. Dyn. Syst. 11(3) (2012) 939–962.
[17] M. Storace, D. Linaro, E. de Lange, The Hindmarsh-Rose neuron model: Bifurcation analysis and piecewise-linear approximations, Chaos 18 (2008) 033128.
[18] A. Sherman, J. Rinzel, J. Keizer, Emergence of organized bursting in clusters of pancreatic β-cells by channel sharing, Biophysical Journal 54 (1988) 411–425.
[19] A. L. Hodgkin, A. F. Huxley, A quantitative description of membrane current and its application to conduction and excitation in nerve, J. Physiol. 117 (1952) 500–544.
[20] A. Shilnikov, M. Kolomiets, Methods of the qualitative theory for the Hindmarsh-Rose model: A case study. a tutorial, Int. J. Bifur. Chaos Appl. Sci. 18(8) (2008) 2141–2168.
[21] J. Rinzel, A formal classification of bursting mechanisms in excitable systems, in: E. Teramoto, M. Yumaguti (Eds.), Mathematical Topics in Population Biology, Morphogenesis and Neurosciences: Proceedings of an International Symposium held in Kyoto, November 10–15, 1985, Springer Berlin Heidelberg, Berlin, Heidelberg, 1987, pp. 267–281.
[22] N. Fenichel, Geometric singular perturbation theory for ordinary differential equations, J. Differential Equations 31 (1) (1979) 53–98.
[23] E. Izhikevich, Dynamical systems in neuroscience. The geometry of excitability and bursting, MIT Press, Cambridge, Mass, 2007.

[24] J. Nowacki, H. M. Osinga, K. Tsaneva-Atanasova, Dynamical systems analysis of spike-adding mechanisms in transient bursts, The Journal of Mathematical Neuroscience 2 (1) (2012) 7.
[25] K. Tsaneva-Atanasova, H. M. Osinga, T. Riess, A. Sherman, Full system bifurcation analysis of endocrine bursting models, Journal of Theoretical Biology 264 (4) (2010) 1133–1146.
[26] A. Shilnikov, G. Cymbalyuk, Transition between tonic spiking and bursting in a neuron model via the blue-sky catastrophe, Physical Review Letters 94 (2005) 048101.
[27] E. Mosekilde, B. Lading, S. Yanchuk, Y. Maistrenko, Bifurcation structure of a model of bursting pancreatic cells, BioSystems 63 (1) (2001) 3–13.
[28] X. Han, Y. Yu, C. Zhang, F. Xia, Q. Bi, Turnover of hysteresis determines novel bursting in duffing system with multiple-frequency external forcings, International Journal of Non-Linear Mechanics 89 (2017) 69–74.
[29] X. Han, Y. Zhang, Q. Bi, J. Kurths, Two novel bursting patterns in the Duffing system with multiple-frequency slow parametric excitations, Chaos 28 (4) (2018) 043111.
[30] D. Terman, Chaotic spikes arising from a model of bursting in excitable membranes, SIAM J. Appl. Math. 51 (5) (1991) 1418–1450.
[31] W. Govaerts, A. Dhooge, Bifurcation, bursting and spike generation in a neural model, Int. J. Bifur. Chaos Appl. Sci. 12 (08) (2002) 1731–1741.
[32] J. Guckenheimer, C. Kuehn, Homoclinic orbits of the FitzHugh-Nagumo equation: the singular-limit, Discrete Contin. Dyn. Syst. Ser. S 2 (4) (2009) 851–872.
[33] J. Guckenheimer, C. Kuehn, Homoclinic orbits of the FitzHugh-Nagumo equation: bifurcations in the full system, SIAM J. Appl. Dyn. Syst. 9 (1) (2010) 138–153.
[34] A. Sherman, J. Rinzel, J. Keizer, Emergence of organized bursting in clusters of pancreatic β-cells by channel sharing, Biophysical Journal 54 (3) (1988) 411 – 425.
[35] E. J. Doedel, R. Paffenroth, A. R. Champneys, T. F. Fairgrieve, Y. A. Kuznetsov, B. E. Oldeman, B. Sandstede, X. J. Wang, Auto2000, http://cmvl.cs.concordia.ca/auto.
[36] A. J. Homburg, B. Sandstede, Homoclinic and heteroclinic bifurcations in vector fields, Handbook of Dynamical Systems 3 (2010) 379–524.
[37] L. Shilnikov, On the birth of a periodic motion from a trajectory bi-asymptotic to an equilibrium state of the saddle type, Soviet Math. Sbornik 35 (1968) 240–264.
[38] A. Champneys, V. Kirk, E. Knobloch, B. Oldeman, J. Rademacher, Unfolding a tangent equilibrium-to-periodic heteroclinic cycle, SIAM J. Appl. Dyn. Syst. 8 (3) (2009) 1261–1304.
[39] T. Chay, J. Keizer, Minimal model for membrane oscillations in the pancreatic β-cell, Biophys J. 42 (2) (1983) 181—190.
[40] A. Sherman, J. Rinzel, Model for synchronization of pancreatic β-cells by gap junction coupling, Biophysical Journal 59 (3) (1991) 547 – 559.